Supramolecular Loading of a Broad Spectrum of Molecular Guests In Hyperbranched Polytriazole Nanoparticles with Cores Containing Multiple Functional Groups

Sasha Padilla-Coley‡, Hui Xu‡, Janeala Morsby, Haifeng Gao, and Bradley D. Smith**

Department of Chemistry and Biochemistry, 251 Nieuwland Science Hall, University of Notre Dame, Notre Dame, Indiana 46556, USA

‡ Contributed equally.

* Corresponding authors. Email: smith.115@nd.edu; hgao@nd.edu

KEYWORDS hyperbranched polymer, unimolecular micelle, supramolecular, fluorescent dye, drug solubility, camptothecin.

ABSTRACT

This study evaluated the supramolecular properties of a new family of water-soluble hyperbranched polytriazoles that have a unimolecular micelle structure. Two new, structurally related hyperbranched polymers (**HBPa** and **HBPn**), with the same size (D_h = 11 nm) and core-shell architecture, were prepared and found to act as nanoscale hosts for a broad spectrum of molecular guests. The globular-shaped hyperbranched polymers were synthesized by a straightforward one-pot polymerization method that permits easy synthetic control of the multiple functional groups within the core. Surrounding the core is a shell of polyethylene glycol chains that promotes solubility in pH 7.4 buffer solution and inhibits self-aggregation of the nanoparticles.

The core of **HBPa**, containing a mixture of anionic carboxylate groups and 1,2,3-triazole rings, could be loaded with cationic hydrophilic (*i.e.*, propidium iodide) or partially hydrophobic (*i.e.*, Hoechst 33342) dyes or drugs, including a binary dye/drug pair (*i.e.*, indocyanine green/mitoxantrone). The core of **HBPn**, containing a mixture of uncharged 2-pentanone chains and 1,2,3-triazole rings, could be loaded with uncharged and very hydrophobic dyes (*i.e.*, Nile Red) or drugs. Improved aqueous solubility of camptothecin was achieved ten-fold from 8.4 ng/mL to 75 ng/mL. Additionally, cell toxicity studies showed that **HBPn** was able to release the camptothecin drug inside A549 cancer cells resulting in increased cell death. Taken together, the results suggest that this new family of water-soluble hyperbranched polytriazoles could be broadly useful as nanocarriers for various applications in therapy, imaging, or a combination of the two (theranostics).

INTRODUCTION

There is a need for biocompatible nanoparticles that can be loaded with guest molecules, such as drugs or fluorescent dyes, and used for applications in biomedicine or nanotechnology.[1] In terms of pharmaceutical science, a biocompatible nanoparticle can improve pharmaceutical efficacy in many ways, including: protecting a pharmaceutical from degradation, promoting mass transport through delivery barriers, and increasing the pharmaceutical residence lifetime at the site of disease.[2] Similarly, nanoparticle loading of fluorescent dyes is known to enhance photophysical properties such as fluorescence brightness and dye photostability which enhances biological imaging performance.[3] Nanoparticles with the capacity to simultaneously host more than one type of guest structure, such as two different drug molecules, or a fluorescent dye and a drug, have promise as sophisticated multicomponent nanocarriers for therapy, imaging, or a combination of the two (theranostics). A particularly attractive attribute of nanoparticles is their

capability to accumulate within solid tumors, a phenomenon that has been attributed to the enhanced permeation and retention (EPR) effect.[4] [5]

Perhaps the best known biocompatible nanoparticles are self-assembled colloids, such as micelles and liposomes (100-1000 nm diameter), that have the capacity to hold many copies of a molecular payload.[6] While self-assembled colloids have many attractive properties, it is hard to fine-tune the payload release kinetics.[7] For example, many self-assembled polymeric micelles undergo undesired breakdown shortly after injection into the bloodstream which can cause a burst of released molecular cargo.[8] This lowers the fraction of payload reaching the target and increases the amount of off-target toxicity.[9] One way to prevent this type of colloid disassembly is to covalently crosslink the self-assembled components and create a unimolecular micelle - a multistep synthetic process that can be effective but whose molecular dispersity can sometimes be hard to reproduce due to the inherently heterogeneous structures.[10] [11] [12] [13] [14] [15] Another way to make a unimolecular micelle is to synthesize a multi-generation dendrimer that either has internal pores large enough to accommodate guest molecules,[16] [17] or alternatively has an exterior surface that can associate with a macromolecular target.[18] [19] [20] [21] [22] Although the perfect, branched structures of dendrimers are aesthetically appealing, they require an iterative series of synthetic steps[23] which makes the production process slow and resource intensive.

The drawbacks with dendrimers have led researchers to consider hyperbranched polymers as more practical alternatives.[24] Hyperbranched polymers have many favorable attributes as potential unimolecular micelles and the capability to make them in a facile one-step polymerization process is extremely attractive. [25] [26] However, the translation of hyperbranched polymer nanoparticles for biomedicine is currently limited by the poorly defined hyperbranched architectures produced by traditional synthesis methods which cannot effectively separate selective polymer-monomer reactions from random monomer-monomer reactions. To date, only a small number of hyperbranched polymers have been partially examined as supramolecular

hosts for molecular payload.[27] Examples include hyperbranched polyglycerols, polyesters and polyphosphates.[28] In each case, the core of the hyperbranched polymer is comprised of only one type of functional group[29] and most often the polymer is used to solubilize hydrophobic drugs in water.[30] A notable limitation with most methods to synthesize hyperbranched polymers is inability to prepare a low-dispersity core composed of a pre-determined mixture of functional groups. Recently, one of our team members (Gao) reported a new and versatile polymerization method that produces well-defined hyperbranched polymer structures with globular shape (proven by TEM).[25 31] The synthetic method is a simple one-pot procedure that employs two sequential Cu-catalyzed azide-alkyne cycloaddition (CuAAC) reactions to first create a hyperbranched polyester-based core and then a poly(ethylene glycol) PEG shell containing a number-average degree of polymerization of 7.5 (Scheme 1).[25 32 33 34 35] The shell of PEG chains promotes solubility in aqueous solution and inhibits self-aggregation of the nanocarriers. The synthetic reactions are straightforward to conduct and there is broad tunability of the polymer size and type of functional groups within the core-shell architecture. This latter attribute has been exploited by incorporating reactive functional groups within the polymer core that permit subsequent covalent attachment of additional molecular components using click chemistry.[31] While these covalent conjugates have many different uses, there are several applications such as payload delivery or sequestration that are more easily achieved by non-covalent association processes with inherently lower activation energies.

Scheme 1. Synthetic route for hyperbranched polytriazole nanoparticles with a poly(AB_2-F) core containing multiple functional groups

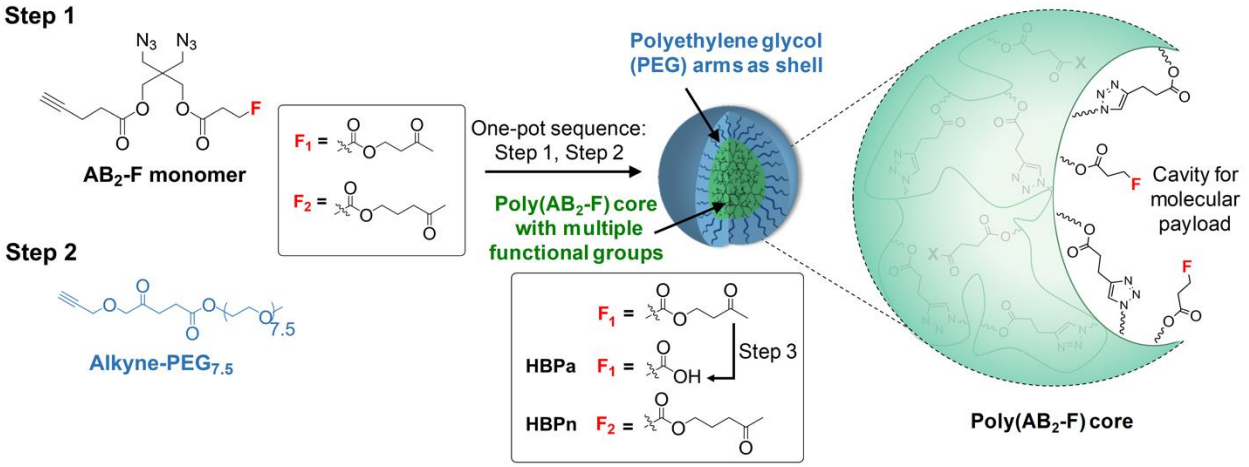

Herein, we disclose the first systematic evaluation of the supramolecular properties of this new hyperbranched polytriazole system. Described below are a series of non-covalent association studies in water that examine two closely related polytriazoles with core-shell architecture. The first hyperbranched polymer is **HBPa** whose core is based on the monomer **AB_2-F_1** with a protected carboxylic acid group that is removed after polymerization. Thus, the core of **HBPa** contains a mixture of anionic carboxylate groups and 1,2,3-triazole rings. The second hyperbranched polymer is **HBPn** whose core is based on the stable monomer **AB_2-F_2** and thus contains a mixture of uncharged 2-pentanone chains and 1,2,3-triazole rings of weak polarity and high lipophilicity. We assess and compare the capabilities of these two novel hyperbranched polymers to associate non-covalently in pH 7.4 buffer solution with three structurally different classes of molecular guests: very hydrophilic cationic fluorescent probes, partially hydrophobic dyes or drugs, and extremely hydrophobic dyes or drugs (Scheme 2). The results demonstrate the supramolecular versatility of this new hyperbranched polytriazole system as a unimolecular micelle platform with broad potential use in various biomedical and nanotechnology applications.

Scheme 2. Molecular guests evaluated for association with the core of hyperbranched polytriazoles in buffer, pH 7.4.

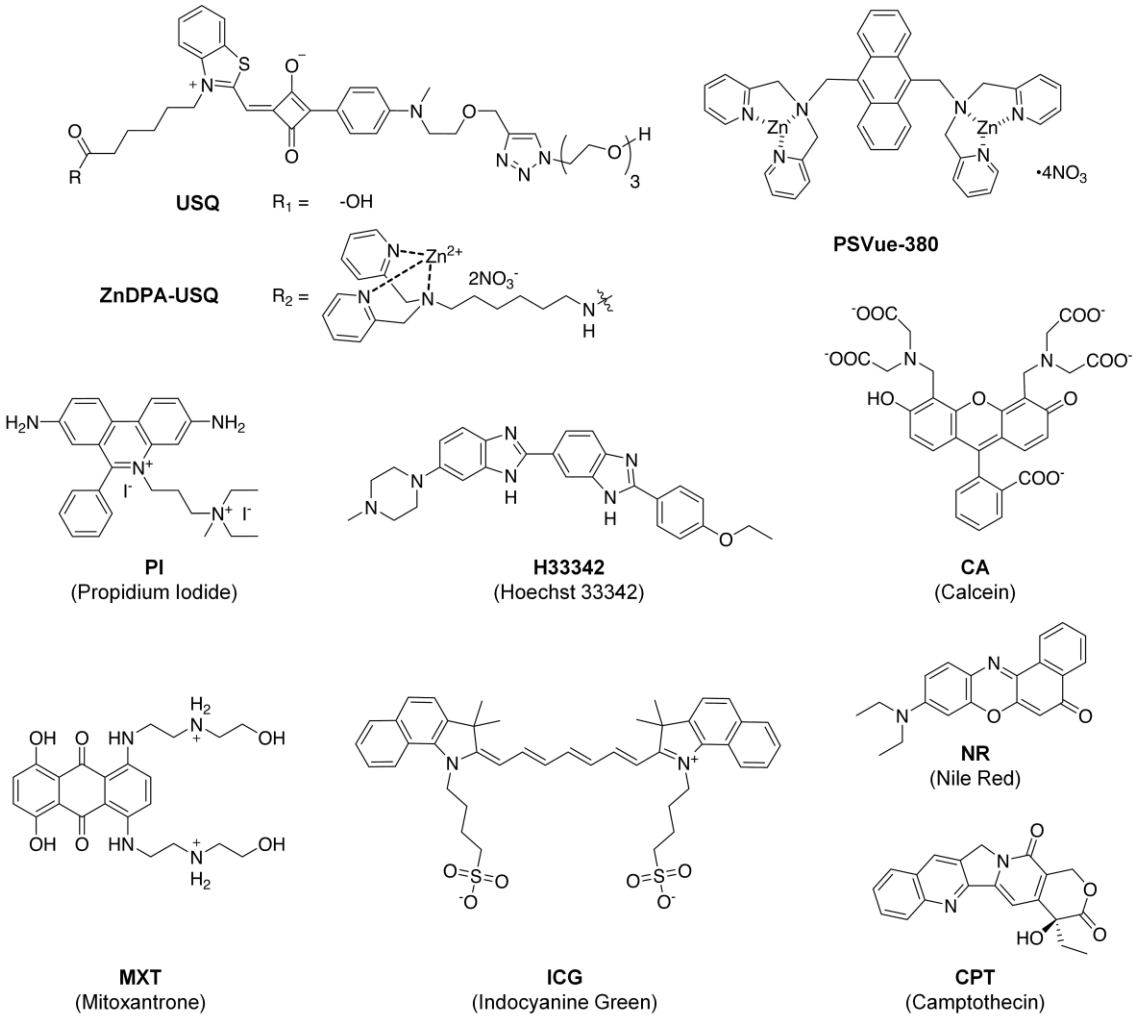

EXPERIMENTAL SECTION

Materials. All chemicals used were reagent grade. Indocyanine green (**ICG**), 2-[4-(2-Hydroxyethyl)piperazin-1-yl]ethanesulfonic acid (HEPES) were obtained from Sigma-Aldrich. The following dyes were purchased from Invitrogen: Nile Red (**NR**), Propidium Iodide (**PI**), and Hoechst 33342 trihydrochloride (**H33342**). (S)-(+)-Camptothecin (**CPT**) was obtained from Tokyo Chemical Industry (TCI) and Mitoxantrone (**MXT**) was purchased from Cayman Chemical

Company (USA) and stored in a freezer at −20 °C. Ascorbic acid (Alfa Aesar, ≥ 99%), copper(II) sulfate pentahydrate ($CuSO_4 \cdot 5H_2O$, BDH, ACS grade), N,N-dimethylformamide (DMF, Sigma-Aldrich , ≥ 99.8%), 2,2'-bipyridyl (bpy, Sigma-Aldrich, ≥ 99%), ethyl ether (EMD Millipore, ≥ 99%), succinic anhydride (TCI America, ≥ 99%), 4-hydroxy-2-butanone (Alfa Aesar, 95%), 5-hydroxy-2-pentanone (TCI America, ≥ 96%). The monomers **AB_2-F_1**, **AB_2-F_2**, and alkynyl-terminated *O*-methyl poly(ethylene glycol) with number-average degree of polymerization = 7.5 (**alkyne-$PEG_{7.5}$**)[36], as well as the central tri-azido core molecule **B_3** (tris((1-(3-azidopropyl)-1H-1,2,3-triazol-4-yl)methyl)amine) were synthesized according to previous literature.[31 32]

Synthesis of hyperbranched polymers. The first step in the one-pot polymerization employed a small amount of tri-azido core molecule **B_3** to initiate the chain-growth polymerization of AB_2-F monomer (**AB_2-F_1** or **AB_2-F_2**). The molar ratio of reactants was $[AB_2\text{-F}]_0$:$[CuSO_4.5H_2O]_0$:[ascorbic acid]$_0$:$[\mathbf{B_3}]_0$ = 350: 10: 40 :1. To achieve this molar ratio, AB_2-F monomer (1.37 mmol), **B_3** (2 mg, 3.9 μmol), $CuSO_4 \cdot 5H_2O$ (9.8 mg, 39.3 μmol) and 2.75 mL DMF were first charged in a 10-mL Schlenk flask with a magnetic stirring bar. The flask was degassed by three freeze-pump-thaw cycles. At the last cycle, the flask was opened when everything was frozen to quickly add ascorbic acid (27.7 mg, 0.157mmol) into the flask before re-capping. The flask was vacuumed and backfilled with N_2 for 3 cycles before immersed in a thermostatic oil bath at 45 °C to thaw the mixture solution and initiate the polymerization.[31] After one hour, the conversion of AB_2-F monomer reached >95%, determined by ^{1}H NMR spectroscopy, and 1.5 molar equivalents of **alkyne-$PEG_{7.5}$** (step 2 of the one-pot sequence) was added under N_2 gas and stirred overnight. The polymerization was stopped by diluting with 5 mL dichloromethane (DCM) and adding four equivalents of bpy ligand to sequester the copper catalyst, then passing through a flash neutral alumina column.[31] After three precipitation cycles using diethyl ether, the pure **HBPn** was obtained (yield: 69%). Production of **HBPa** followed the same polymerization sequence with a deprotection step (step 3) to remove the carboxylate protecting group. The purified protected form

of **HBP** (800 mg, 0.83 mmol) from polymerization of **AB_2-F_1** was dissolved in DCM and treated with triethylamine (DCM/TEA=4:1, v/v, 5mL), followed by stirring overnight. DCM was added to the reaction solution, which was washed three times each with 1 M HCl solution and brine solution. Rotary evaporation of the dried organic phase provided pure **HBPa** (Scheme 1). Inductively coupled plasma-optical emission spectrometry (ICP-OES) characterization of the samples confirmed that Cu residue amount was about ~10 ppm.

Characterization of hyperbranched polymers. The hydrodynamic diameter (D_h) of polymers was determined in aqueous solution by dynamic light scattering (DLS, Zetasizer Nano ZS). The apparent number-average molecular weight (M_n) and polydispersity (M_w/M_n) were determined by size exclusion chromatography (SEC) with DMF as the mobile phase based on linear poly(methyl methacrylate) (PMMA) standards, which was equipped with a Waters 515 HPLC pump, Polymer Standards Services (PSS) columns (GRAM, 10^4, 10^3, and 10^2 Å) at 55 °C with DMF flow rate = 1.00 mL min^{-1}, a Waters 2414 RI detector. Proton nuclear magnetic resonance (^{1}H NMR) spectroscopy was acquired on a Bruker 500 MHz spectrometer at 25 °C using $CDCl_3$ or DMSO-d_6 as solvent. FT-IR was conducted using a Thermo Nicolet IR 200 spectrometer equipped with a deuterated triglycine sulfate (DTGS) detector, mid-IR source (4000–400 cm^{-1}) and Ge on KBr beam splitter.

Non-covalent loading studies. *Aqueous loading of hydrophilic dyes or drugs:* The hyperbranched polytriazole (**HBPa** or **HBPn**) and hydrophilic molecular guest were simply mixed at appropriate molar ratios in aqueous buffer. *Organic loading of hydrophobic dyes or drugs.* A tetrahydrofuran (THF) solution containing hyperbranched polytriazole (**HBPa** or **HBPn**) and hydrophobic molecular guest were evaporated using a rotary evaporator and the residual film dried overnight under high vacuum line to ensure complete removal of the solvent. The film was reconstituted in aqueous buffer and any undissolved solid was removed by centrifugation. The extreme insolubility of CPT allows this simple method to eliminate CPT not bound within a

nanocontainer. Guest solubilization in water due to loading within the polymer core was confirmed by absorption and fluorescence spectroscopy.

Supramolecular studies. *Fluorescence titrations*. All measurements were made in triplicate. A solution of 2 μM guest in 20 mM HEPES buffer solution (pH 7.4) was placed in a 1 mL quartz cuvette and titrated with aliquots from a hyperbranched polymer stock solution (0.8 mM **HBPa**, M_n 65,900). A fluorescence scan was obtained after each addition of polymer and fluorescence measurements at a single point were plotted to produce an isotherm that was fitted to a 1:1 binding model using the algorithm described in the Supporting Information. Also provided in the Supporting Information are algorithms used for measurement of fluorescence polarization, FRET (Förster Resonance Energy Transfer) efficiency, and the determination of **CPT** solubilization and polymer loading efficiency.

Cell studies. *Sample preparation.* Stock solutions of polymer (**HBPa** or **HBPn**) were prepared at 0.8 mM concentrations in HEPES buffer (pH 7.4). Solutions were then filtered using a 0.1 μm filter prior to conducting experiments to remove any dust or undesired large aggregates.

Cytotoxicity studies. *To* 96-well plates, CHO-K1 cells were seeded at a density of 3000 cells/well. Cells were treated with varied concentrations of sample a day later followed by a 24-hour incubation period. After treatment cells were subjected to an MTT assay using standard protocols. Absorbance readings were measured at 570 nm.

General microscopy methods. CHO-K1 cells were grown to 80% confluency on 8-well chambered cover glass slides. Separate samples containing an equal number of cells were incubated with 100 μL of **HBPn** alone (0.5 mg/mL), **CPT** alone (4.2 ng/mL), or a formulation of **HBPn•CPT** (0.5 mg/mL, 37.5 ng/mL) diluted in F12K media for 3 hours at 37 ^{o}C. The cells were washed three times with PBS containing Ca^{2+} and Mg^{2+} followed by fixation with cold 4% paraformaldehyde for 20 minutes at room temperature. The cells were washed again and imaged under fresh PBS using a GE Healthcare DeltaVision Deconvolution fluorescence microscope

equipped with an X-cite 120 fluorescence illumination system. Images were collected in softWoRx using a CoolSNAP_HQ2 camera operating in CCD mode with a 1 MHz readout speed. A DAPI filter set (Ex: 360/40 nm, Em: 457/50 nm) was used with 5 second acquisition times. Images were processed using ImageJ software and scaled to the highest intensity image in the set.

RESULTS AND DISCUSSION

Polymer synthesis and characterization. As illustrated in Scheme 1, the hyperbranched polymer synthesis employed a one-pot, two-step sequence of CuAAC reactions that first induced chain-growth polymerization of an AB_2-F monomer (**AB_2-F_1** or **AB_2-F_2**) in DMF to construct a hyperbranched polytriazole core (Step 1), and then attachment of alkyne-$PEG_{7.5}$ chains to introduce a PEG shell (Step 2).[31] The molar ratio of reactants in step 1 was $[AB_2\text{-}F]_0$:$[CuSO_4.5H_2O]_0$:[ascorbic acid]$_0$:$[\mathbf{B_3}]_0$ = 350: 10: 40 :1 in DMF at 45 °C. After the polymerization reaction was > 95% complete (determined by ^{1}H NMR spectroscopy), an aliquot containing 1.5 molar equivalents of **alkyne-$PEG_{7.5}$** was added to the same pot and the reaction monitored by FT-IR until >95% of the azide groups were observed to be consumed (Figure S1). To produce **HBPa**, trimethylamine was used as a weak base to promote a clean β-elimination reaction that removed the carboxylate protecting group within the F_1 structure (Step 3), a chemical process that was easily monitored by ^{1}H NMR spectroscopy (Figure S2).[37] SEC characterization of **HBPa** revealed a structurally defined hyperbranched polymer with apparent number-average molecular weight M_n = 65,900 and polydispersity M_w/M_n = 1.05, (Figure 1a). DLS measurements showed that the hydrodynamic diameter was about D_h = 10.7 nm in deionized water and the nanoparticle size did not change with time at neutral or acidic pH (Figure 1c). Samples of **HBPn**, prepared by the same one-pot two-step procedure were found to be structurally very similar with M_n = 73,700, polydispersity of M_w/M_n = 1.05, and hydrodynamic diameter about D_h = 11 nm in deionized water (Figures 1a-b). Thus, the synthetic chemistry produced the two analogous water-soluble

hyperbranched nanoscale polymers **HBPa** and **HBPn** with virtually the same particle size and polydispersity. The only difference is identity of the functional groups within the core of the polymeric nanoparticles; with **HBPa**, it is a mixture of anionic carboxylate groups and 1,2,3-triazole rings, and with **HBPn** it is a mixture of uncharged 2-pentanone chains and 1,2,3-triazole rings. These two polymer nanoparticles were subsequently tested for capability to associate non-covalently with the molecular guests shown in Scheme 2.

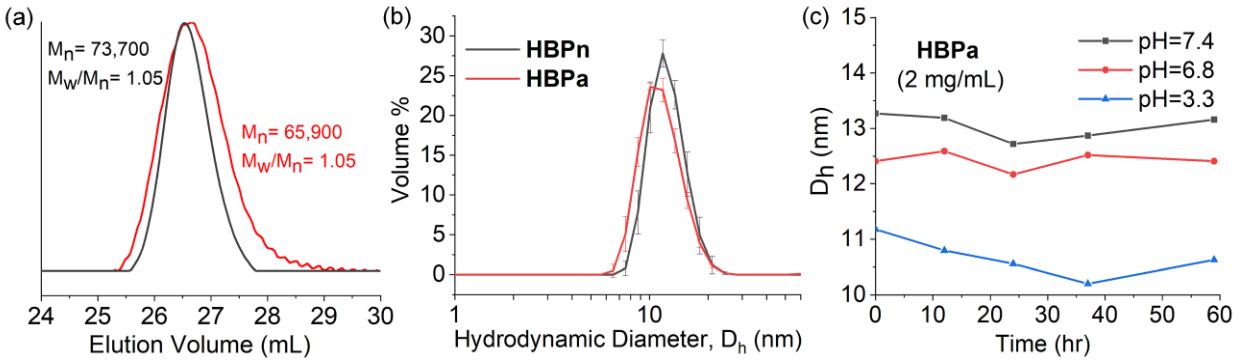

Figure 1. (a) Representative SEC traces of purified polymers in DMF. (b) DLS measurements of purified polymers (2 mg/mL) in deionized water at 25 ºC. (c) Change in hydrodynamic diameter over time.

Loading of hyperbranched polymer with hydrophilic cationic guests. The first goal of the guest association studies was to determine if **HBPa**, the hyperbranched polymer with an anionic carboxylate-containing core, could be loaded with water-soluble fluorescent probes that are known to have carboxylate affinity. We used **PSVue380** and **ZnDPA-USQ**, two zinc-based fluorescent probes that exhibit enhanced fluorescence when they associate with polyoxyanions.[38] [39] Shown in Figure 2 are the changes in probe fluorescence for separate samples after addition of the two polymers. The same fluorescence effect was observed with both probes; that is, negligible change in fluorescence when **HBPn** was added to the probes, but a large increase in probe fluorescence after addition of **HBPa** (Figure 2; Figure S3). The increase in fluorescence

enabled titration studies that measured probe affinity for **HBPa**. Interestingly, the titration isotherms (Figure S4) fitted nicely to a 1:1 (probe:**HBPa**) binding model and K_a values of 2.1 x 10^6 M^{-1} and 1.1 x 10^6 M^{-1} were determined for **PSVue380** and **ZnDPA-USQ,** respectively (Figure S4). These K_a values are larger than literature values for polycarboxylate binding in water by similar ZnDPA probes,[40] and suggest that the core of **HBPa** contains; (a) a high local concentration of carboxylate groups, and (b) a probe binding site whose microenvironment is less polar than bulk water (see below for supporting data) and thus enhances electrostatic attraction. Two control experiments produced results that were consistent with a binding model dominated by electrostatic interactions; (a) affinity of **PSVue380** and **ZnDPA-USQ** probes for **HBPa** was lost when the Zn^{2+} cations within the probe structures were sequestered by adding the Zn^{2+}-chelator ethylenediaminetetraacetic acid (EDTA, Figure S5), (b) there was no evidence of polymer/dye association (i.e., no change in dye fluorescence) when **HBPa** or **HBPn** was added to separate solutions of the anionic fluorescent dyes **USQ** (Figure S6) or **calcein** (Figure S7). We conclude that strong electrostatic interactions drive association of the cationic zinc-based fluorescent probes, **PSVue380** and **ZnDPA-USQ**, with the anionic core of **HBPa**.[41] In contrast, the two hydrophilic zinc-based cationic fluorescent probes have no apparent affinity for the uncharged lipophilic core of **HBPn**.

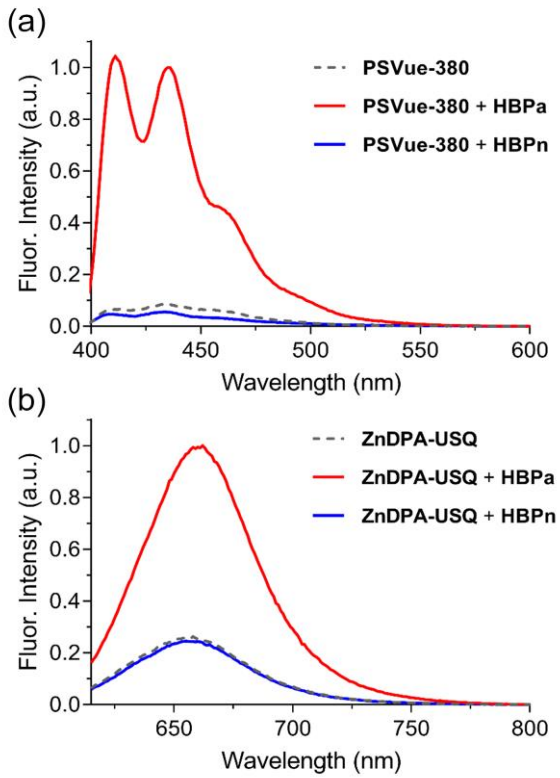

Figure 2. Fluorescence emission spectra of 2 μM (a) **PSVue 380** and (b) **ZnDPA-USQ** in the absence or presence of excess **HBPa** or **HBPn** in 10 mM HEPES buffer solution (pH 7.4).

Loading of hyperbranched polymer with partially hydrophobic cationic guests. In addition to carboxylate groups, the core of **HBPa** also contains 1,2,3-triazole rings that can potentially stack against guest molecules that have aromatic surfaces and provide stabilizing intermolecular interactions.[42,43] Thus, we hypothesized that organic guest structures containing a combination of positive charge and partially hydrophobic aromatic surfaces would have good affinity for the core of **HBPa**.

To test this proposal, we determined if the core of the hyperbranched polymers could be loaded with the planar cationic dyes **PI** (propidium iodide) and **H33342** (Hoechst 33342). Both compounds are fluorescent dyes known to exhibit enhanced emission when they form intercalated complexes with double-stranded DNA.[44,45] Shown in Figure 3 are the absorption and emission

spectra for separate solutions of **PI** before and after addition of the two hyperbranched polymers. Addition of **HBPn** produced no changes in the **PI** spectra, but addition of **HBPa** induced a red-shift in absorbance and a doubling of the probe's red fluorescence that was easily visible to the naked eye. As above, fluorescence titration experiments produced a titration isotherm (Figure S8) that matched a 1:1 binding model with an apparent K_a of 2.7 x 10^6 M^{-1} for association of **PI** and **HBPa** (Figure S8). The structure of **PI** has a permanent positive charge of +2, suggesting that electrostatic interactions are a major factor favoring affinity of **PI** for the anionic core of **HBPa**. Evidence for this conclusion was gained by a titration experiment that incrementally added Ca^{2+} to a mixture of **PI** + **HBPa** and found that the Ca^{2+} ions immediately displaced the **PI** from the hyperbranched polymer into the bulk water (Figures 4; Figure S9). This is an important result for two reasons. First, it shows that a molecular guest can be released from the core of the hyperbranched polymer nanocarrier. Moreover, the rapid Ca^{2+} triggered release of the **PI** indicates that the loaded **PI** is not buried deep inside the core of **HBPa** but rather it is held in shallow cavities that can be readily accessed by the added Ca^{2+}.

An analogous set of absorption and fluorescence experiments was conducted with **H33342**, a basic dye molecule whose protonation state depends on the pH of microenvironment.[46] [47] [48] Previous work has shown that DNA intercalation by **H33342** is driven primarily by hydrophobic effects.[48] As shown in Figure 3, addition of **HBPn** to a solution of **H33342** produced a red shift in absorption and enhanced fluorescence emission, with an even larger optical change produced by addition of **HBPa**. A fluorescence titration experiment that added aliquots of **HBPa** to a solution of **H33342** measured an apparent K_a of 1.2 x 10^5 M^{-1} (Figure S8), and a solution containing the complex of **H33342** + **HBPa** was found to be stable upon storage at 4 ºC (Figure S10). Competitive titration experiments that added Ca^{2+} ions to a binary mixture of **H33342** + **HBPa** produced no changes in **H33342** spectra (Figure S11) indicating no ejection of the **H33342** from the polymer core. Together, these results suggest that hydrophobic stacking with the triazoles is

the primary factor controlling the polymer loading and release of **H33342**,[42] [43] with stabilizing electrostatic interactions having an important but secondary role.[49]

A summary of measured association constants for binding of fluorescent cationic molecular guests by **HPBa** is provided in Table 1. Although the values of K_a only differ by a factor of twenty, it is important to realize that there is a major change in the supramolecular interactions that determine the extent of guest association with the core of **HPBa** that contains both anionic carboxylate groups and triazole rings. Favorable electrostatics drives the loading of hydrophilic cationic guests (**PSVue380**, **ZnDPA-USQ**, and **PI**), whereas, hydrophobic stacking with the triazole rings in the polymer core is the main factor for association of **H33342**. While there is no doubt that the guests associate with the core of the hyperbranched polymers, the precise location of the binding sites within the core is less clear. The rapid guest association kinetics observed throughout the study suggests that the bound guests likely reside in cavities near the core-shell interface as shown in Scheme 1. One of the future research goals is to increase the internal porosity of the poly(AB_2-F) core by revising the polymer synthesis to include AB_2-F monomers that have long rigid spacers between the A and B_2 groups.

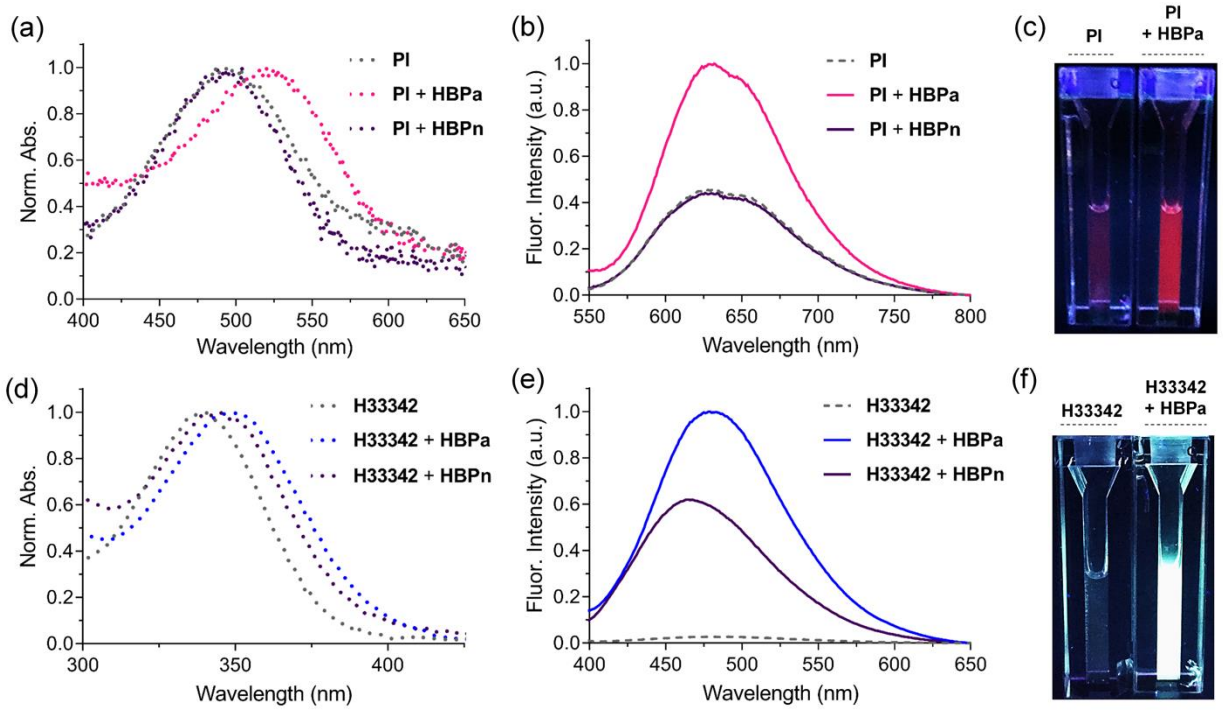

Figure 3. (a,d) Absorbance and (b,e) fluorescence emission spectra of 2 μM **PI** (propidium iodide) or **H33342** (Hoechst 33342) and the absence or presence of excess (24 μM) **HBPa** or **HBPn** in 10 mM HEPES buffer solution, pH 7.4 ($\lambda_{ex\ PI}$ = 496 nm, $\lambda_{ex\ H33342}$ = 350 nm; slits 5 nm). (c,f) Photographs of cuvettes, illuminated under hand-held long-wave UV lamp, containing **PI** (c) or **H33342** (f) before (*left*) and after (*right*) addition of **HBPa.**

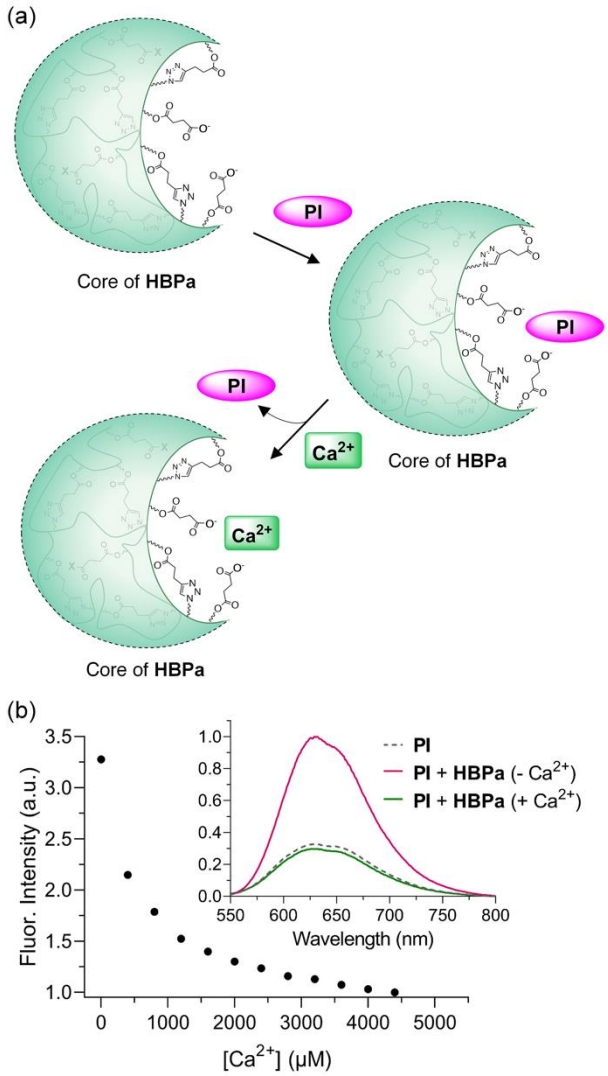

Figure 4. (a) Schematic representation of Ca^{2+} displacement of **PI** from the core of **HBPa**. (b) Fluorescence titration isotherm (λ_{ex} = 496 nm, λ_{em} = 631 nm) indicating displacement of **PI** from **HBPa** upon incremental addition of aliquots of $CaCl_2$, in 10 mM HEPES buffer at pH 7.4. The insert shows fluorescence emission spectra for free **PI** (2 μM) and a binary mixture of **PI** (2 μM) + **HBPa** (24 μM) in the presence and absence of 12 mM Ca^{2+}.

Table 1. Association constants (K_a) for various dyes and **HBPa** in 10 mM HEPES buffer (pH 7.4) at 25 °C.

Entry	Guest Molecule	K_a (M^{-1})
1	**PSVue-380**	(2.1 ± 0.9) x 10^6
2	**ZnDPA-USQ**	(1.1 ± 0.1) x 10^6
3	**H33342**	(1.2 ± 0.5) x 10^5
4	**PI**	(2.7 ± 1.1) x 10^6

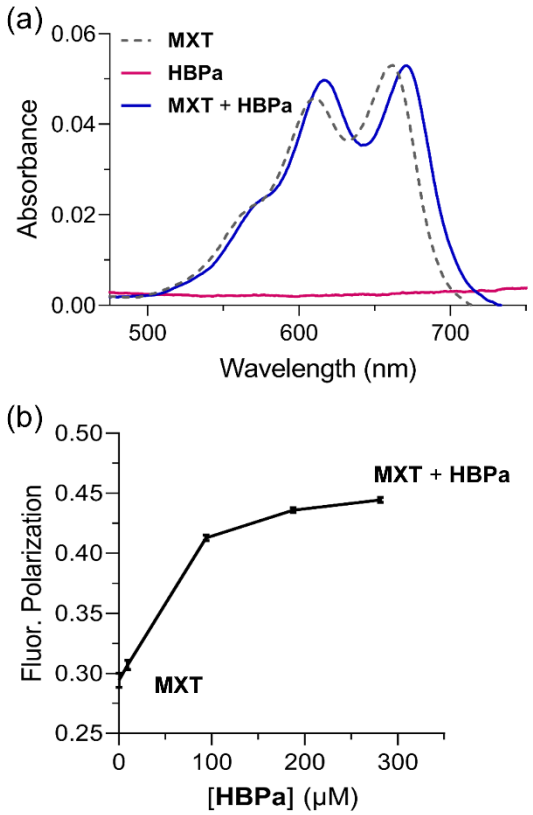

Figure 5. (a) Absorbance spectra of **MXT** (mitoxantrone, 15 μM) before and after the addition of excess **HBPa**. Control experiment using **HBPa** showed no absorption (pink line) or fluorescence emission (data not shown). (b) Fluorescence polarization titration experiment (λ_{ex} = 610, λ_{em} = 683 nm) that incrementally added **HBPa** to a solution of **MXT** (15 μM). All in 10 mM HEPES buffer (pH 7.4).

In addition to the above binding studies using fluorescent dyes, we investigated hyperbranched polymer association at pH 7.4 with the cationic anthraquinone drug **MXT** (mitoxantrone) which is easily studied because it exhibits deep-red absorption and moderate fluorescence emission bands.[50] We observed that addition of **HBPa** induced a red shift in the **MXT** absorption band and a distinct increase in its fluorescence polarization value (Figure 5), indicating association of **MXT** with the hyperbranched polymer. The change in spectral features induced by **MXT** binding was not large enough to accurately determine a binding constant or a binding stoichiometry. But an attractive property of **MXT** is its capacity to act as a FRET (Förster resonance energy transfer) energy donor when confined in close space near an energy acceptor that provides appropriate spectral overlap.[51] [52] We exploited this property by devising a FRET experiment to determine if the core of **HBPa** could be simultaneously loaded with two different guest structures in close proximity. As shown in Figure 6, we employed **MXT** as a FRET donor and the near-infrared fluorescent dye **ICG** (indocyanine green) as a FRET acceptor. Absorption and fluorescence spectra were acquired for solutions of **HBPa** mixed with **MXT** or **ICG** alone, and **HBPa** mixed with a 1:1 combination of **MXT** and **ICG**. The spectra in Figure S12 show that the presence of **HBPa** induces red shifts in the absorption and fluorescence bands of **ICG** alone or **MXT** alone, indicating guest association with the core of **HBPa**. The spectra in Figure 5a reflect efficient FRET when **HBPa** was mixed with a 1:1 combination of **MXT** and **ICG**. There is a large decrease in fluorescence intensity for the **MXT** donor at 684 nm, and a corresponding increase in fluorescence intensity of the **ICG** acceptor at 813 nm. Quantitative analysis determined a FRET efficiency of 36.6% (see Supporting Information), strongly supporting the conclusion that the anionic core of **HBPa** can accommodate a binary complex of **ICG**:**MXT** that has a net charge of +1. Based on these results, there is little doubt that the core of **HBPa** could be loaded with a wide range of cationic anthraquinone drugs that are structurally similar to **MXT** such as doxorubicin and pixantrone,[53] as well as suitable drug/dye pairs that can be used for studies of pharmaceutical

release kinetics or theranostic strategies that combine chemotherapy with a phototherapeutic effect.[54]

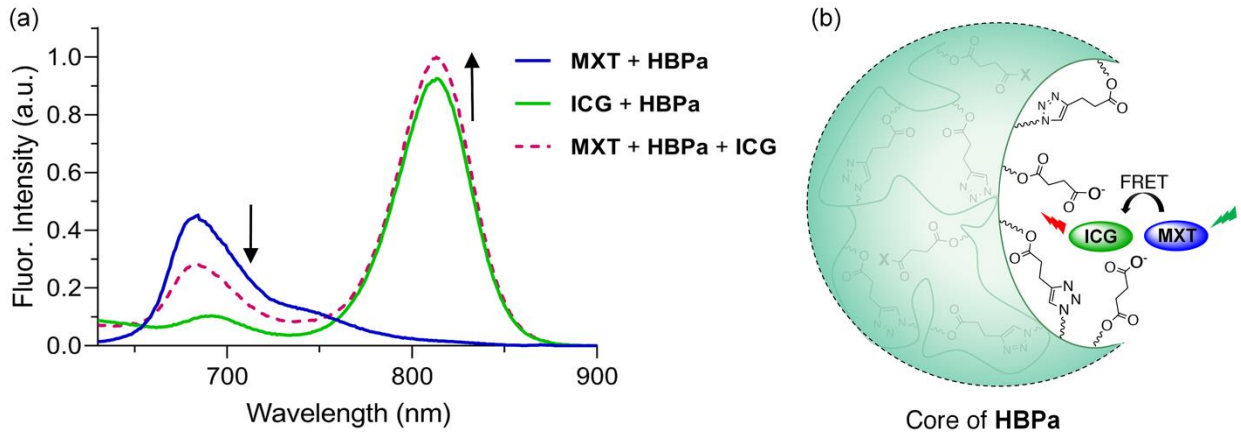

Figure 6. FRET exhibited by **MXT** (energy donor at 684 nm) and **ICG** (energy acceptor at 813 nm) when encapsulated within the core of **HBPa.** (a) Fluorescence emission spectra of **MXT** and **ICG** in the absence or presence of **HBPa** (λ_{ex} = 580 nm; slits 5 nm). All in 10 mM HEPES buffer (pH 7.4). (b) Schematic representation of the FRET process enabled by the simultaneous loading of **ICG** and **MXT** within the core of **HBPa**.

Hyperbranched polymer loading of extremely hydrophobic guests. The capability of the two hyperbranched polymers to act as water-soluble nanocarriers for insoluble dyes or drugs was assessed by conducting a series of aqueous solubilization studies. The first set of solubilization studies used **NR** (Nile Red), a solvatochromic dye with very low solubility in water.[55] Attempts to directly solubilize a film of **NR** with an aqueous solution of hyperbranched polymer (aqueous loading) were not successful. Therefore, we employed an alternative method (organic loading) that evaporated a THF solution of the two components (**NR** and hyperbranched polymer) to create a thin film that was subsequently dispersed into a solution of HEPES buffer (pH 7.4). Spectral analysis of the dispersed solution clearly indicated solubilization of the **NR** by **HBPn** and **HBPa** (Figure 7) with moderately higher loading by the **HPBn**. Moreover, there was a distinct difference

in fluorescence emission wavelengths for the polymer-bound **NR**, reflecting a difference in polarity of the polymer cores. More specifically, the **NR** fluorescence emission wavelengths were 622 nm and 647 nm for **NR** within the cores of **HBPn** and **HBPa**, respectively. A comparison of **NR** emission wavelengths in different solvents (Figure S13) yields results that are consistent with structural model in Scheme 1. That is, the core of **HBPa** has a polarity that is close to methanol, whereas the core of **HBPn** is less polar and close to that of the aprotic organic solvent DMF.[56] This agrees with the general picture that the core of **HBPa** is significantly more polar than the core of **HBPn**.

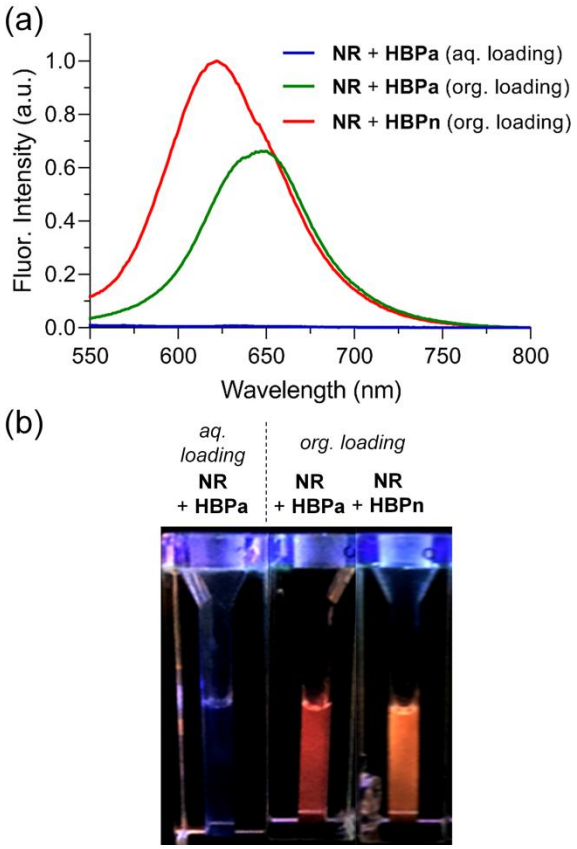

Figure 7. (a) Fluorescence emission spectra (λ_{ex} = 520 nm) of 2 μM **NR** (Nile Red) in the presence of 40 μM **HBPa** or **HBPn** in 20 mM HEPES (pH 7.4) using different solubilization methods (aq. loading or organic loading). (b) Photographs of cuvettes, illuminated by a hand-held long-wave

UV lamp: (from *left* to *right*) **NR** + **HBPa** (aq. loading), **NR** + **HBPa** (org. loading), **NR** + **HBPn** (org. loading).

A second set of solubilization studies examined camptothecin (**CPT**) a well-known topoisomerase I inhibitor that is used to treat many types of cancer including leukemia, liver, lung, and bladder cancers.[57] The pharmaceutical limitations of **CPT**, such as very poor aqueous solubility, susceptibility to degradation, and severe systemic toxicity, have motivated many studies to develop improved formulations.[58] We reasoned that **CPT** could be water-solubilized by **HBPn** using an organic loading method. Thus, a mixture of **CPT** and **HBPn** in THF was evaporated and the residual film dispersed into HEPES buffer solution, followed by several centrifugation cycles to remove any drug that was not solubilized. **CPT** is a fluorescent molecule and as shown by the absorption and fluorescence spectra in Figures 8a-b, the **HBPn** significantly increased the amount **CPT** in aqueous solution. Qualitatively, the fluorescence emitted by the additional **CPT** in solution could be readily visualized by simply illuminating the sample with a hand-held lamp (Figure 8c). Quantitative measurements found the drug loading efficiency to be 0.22% with a ten-fold improvement in aqueous solubility from 8.4 ng/mL,[59] to 75 ng/mL (see Supporting Information).

The next step was to determine if a formulation of **HBPn•CPT** enhanced delivery of **CPT** into cells and induced a higher toxic effect. The cell studies employed cultured Chinese hamster ovary (CHO-K1) cells as a convenient cell model. Cytotoxicity was measured using a standard MTT assay that treated separate samples of cells for 24 hours with **HBPn** alone, **CPT** alone, and a formulation of **HBPn•CPT**. As shown in Figure 8d, treatment with the formulation of **HBPn•CPT** reduced cell viability to about 30%, whereas treatment with molar equivalents of **HBPn** alone or **CPT** alone produced negligible cell toxicity. Additionally, cell toxicity of empty nanocarriers was further evaluated and showed no acute toxicity at varying concentrations (Figure S14). Fluorescence microscopy experiments provided evidence for increased cell uptake of **CPT** by

cells that were treated with the formulation of **HBPn•CPT**. The micrographs in Figure 8e are consistent with uptake of **HBPn•CPT** by endocytosis. The fact that the **HBPn•CPT** treatment is cytotoxic implies that a significant amount of **CPT** is able to escape the endosomes and also the confines of the **HBPn** nanocarriers to gain access to the intracellular topoisomerase enzymes. This is an important finding because drug release from the nanocarrier is a necessary attribute of any successful drug delivery vehicle.

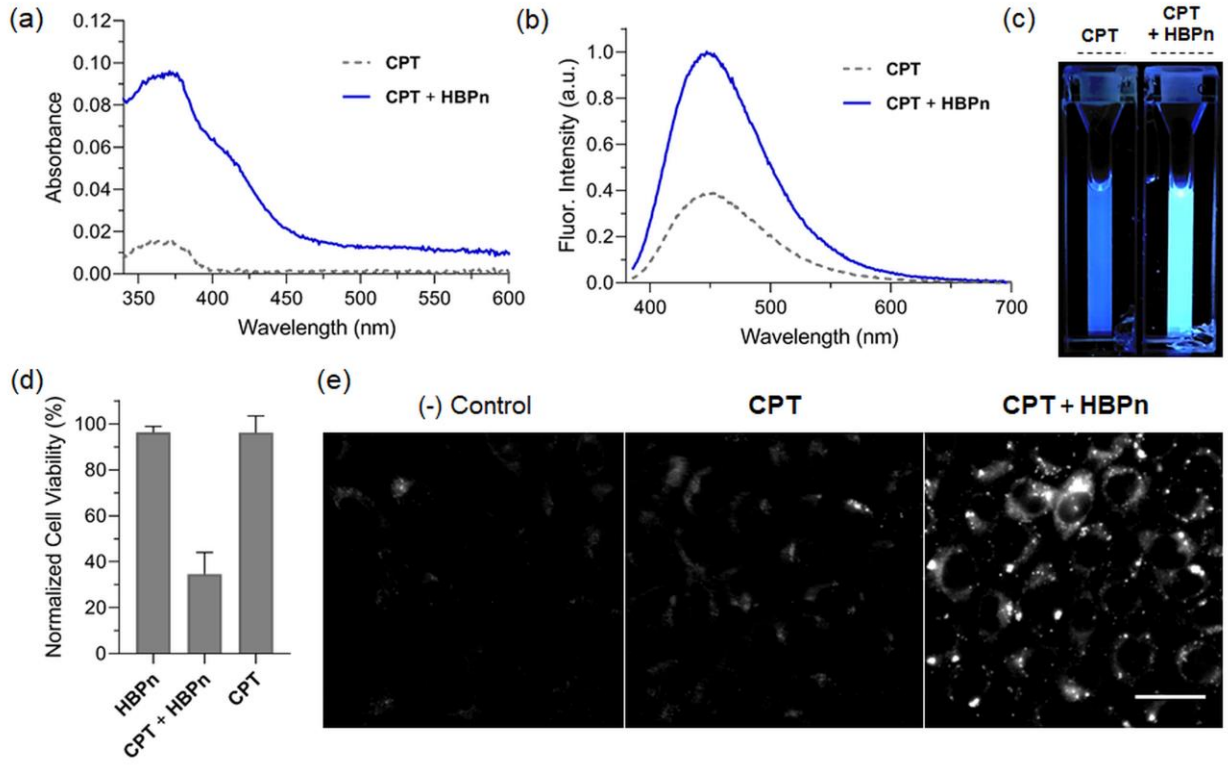

Figure 8. (a) Absorbance and (b) fluorescence emission spectra of **CPT** (camptothecin) in the absence or presence of **HBPn** in 20 mM HEPES buffer solution, pH 7.4 ($\lambda_{ex\ CPT}$ = 370 nm; slits 1 nm). (c) Photographs of cuvettes, illuminated under hand-held long-wave UV lamp, containing **CPT** in the absence (*left*) and presence (*right*) of **HBPn**. (d) Cell viability of CHO-K1 cells after incubation for 24 hours with equal molar **HBPn** alone (0.5 mg/mL), **CPT** alone (4.2 ng/mL), or a formulation of **HBPn•CPT** (0.5 mg/mL, 37.5 ng/mL). (e) Fluorescence micrographs (DAPI filter

set: λ_{ex} = 360/40 nm, λ_{em} = 457/50 nm) of CHO-K1 cells treated for 3 hours with **CPT** alone or a formulation of **HBPn•CPT** followed by fixation with 4% paraformaldehyde (scale bar = 21 μm).

CONCLUSIONS AND FUTURE DIRECTIONS

Supramolecular studies of globular hyperbranched polymers in water are quite rare,[27 28 29 30] which is surprising since unimolecular micelles have long been considered as potential nanocarriers. This study compared two closely related hyperbranched polytriazoles (**HBPa** and **HBPn**) with the same core-shell architecture, globular shape (hydrodynamic diameter D_h ~11 nm), molecular weight (M_n = 65,000-75,000), and surrounding hydrophilic shell of PEG chains. When viewed from an external perspective, the polymer nanoparticles are structurally reminiscent of average-size, water-soluble eukaryotic proteins. Both polymers were prepared by a straightforward one-pot polymerization method that permits synthetic control of the mixed functional groups within the core of the hyperbranched nanoparticles (Scheme 1). A battery of supramolecular studies in pH 7.4 buffer showed that the core of **HBPa** or **HBPn** can be loaded with a broad spectrum of molecular guests. The carboxylate groups within the core of **HBPa** induce a relatively polar microenvironment that favor electrostatic association with hydrophilic cationic molecular guests and even divalent cations such as Ca^{2+}. In addition to the carboxylates, the core of **HBPa** contains 1,2,3-triazole rings which promote aromatic stacking, and permits reversible association of cationic but partially hydrophobic drugs and dyes. Thus, **HBPa** is a versatile unimolecular micelle that can be reversibly loaded with a wide range of cationic guest molecules with structures that vary from highly hydrophilic to partially hydrophobic molecules (Scheme 2). The ability to load different fluorescent dye and drug structures that have a wide range of emission wavelengths and photostabilities means that the biodistribution of the same hyperbranched polytriazole system can be imaged over vastly different length scales in different biological systems using modern fluorescence microscopy or in vivo imaging methods. Moreover,

the ability to load a binary fluorescent near-infrared drug/dye mixture as a FRET pair creates a powerful experimental platform for future imaging studies of guest release from **HBPa** inside cells or living subjects.[60] In addition, polymer loaded drug/dye pairs have great promise as theranostic agents that combine fluorescence imaging, chemotherapy, and near-infrared phototherapy.[54] In contrast to **HBPa**, the core of **HBPn** contains uncharged functional groups and a less polar microenvironment that favors loading of hydrophobic drugs or dyes. Notably, **HBPn** promotes water solubilization of extremely hydrophobic drugs such as **CPT** and subsequent delivery into cells. The empty **HBPn** is not toxic to cells but a **CPT**-loaded version is taken up by cell endocytosis (as proved by fluorescence imaging) leading to intracellular **CPT** release from the nanocarrier followed by inhibition of topoisomerase and enhanced chemotherapeutic efficacy. This result illustrates the theranostic capabilities of the hyperbranched polytriazole to deliver and release drugs inside cells and also permit simultaneous tracking of the process by fluorescence imaging.

A major potential advantage of the core-shell architecture is the capability to fine-tune the size and structure for optimized biodistribution. In this regard, it is becoming increasingly apparent that the structural factors that affect the biodistribution and blood clearance of soft nanoparticles are multifarious and context specific.[61] Recent studies with PEGylated nanoparticles have found systems with Dh close to 11 nm that can accumulate in tumors due to an apparent EPR effect and yet still be excreted by the renal pathway.[5] This may be due in part to the inherent ability of soft materials to extravasate through constricted biological openings without structural disintegration.[62] The core-shell architecture of hyperbranched polytriazoles and modular synthetic method makes it easy to control particle size and thickness of PEG shell. For instance, we have previously demonstrated that the change of monomer to core feed ratio from 100 to 2700 could effectively tuned the hydrodynamic size of nanoparticles from 6.5 nm to 25

nm.[25] Thus, there is wide structural scope to explore in order to achieve a desired biodistribution outcome.

Because of the relatively small size (Dh ~11 nm) the loading capacity of these hyperbranched polytriazoles is low which is typical for unimolecular micelles.[62] However, it should be possible to increase the guest loading capacity of these polymers by employing AB_2-F monomers that have long rigid spacers between the A and B_2 groups. This will lead to hyperbranched polymer with large internal pores that can accommodate many copies of molecular payload. Furthermore, it should be straightforward to further enhance the supramolecular performance by introducing prosthetic groups into the core using robust post-polymerization functionalization methods based on click chemistry.[31] Taken together, the results suggest that this new family of hyperbranched polytriazoles will be broadly useful as a new nanoscale platform for easy conversion into multifunctional nanocarriers for various applications in therapy, imaging, or a combination of the two (theranostics).

ASSOCIATED CONTENT

Supporting Information

The Supporting Information is available free of charge at https://pubs.acs.org/doi/.

Polymer characterization, guest association data, and data manipulation algorithms (PDF)

AUTHOR INFORMATION

Corresponding Authors

* Email: hgao@nd.edu, smith.115@nd.edu

ORCID

Bradley D. Smith: 0000-0003-4120-3210

Haifeng Gao: 0000-0001-9029-5022

Sasha Padilla-Coley: 0000-0002-5146-170X

Notes

The authors declare no competing financial interest

ACKNOWLEDGMENTS

We are grateful for funding support from the National Science Foundation (CHE-1554519, CHE-1708240), and the National Science Foundation Graduate Research Fellowship Program (DGE-1841556). Any opinions, findings, and conclusions or recommendations expressed in this material are those of the authors and do not necessarily reflect the views of the funding agencies.

REFERENCES

(1) Ting, J. M.; Porter, W. W.; Mecca, J. M.; Bates, F. S.; Reineke, T. M. Advances in Polymer Design for Enhancing Oral Drug Solubility and Delivery. *Bioconjugate Chem.* **2018**, *29* (4), 939–952. https://doi.org/10.1021/acs.bioconjchem.7b00646.

(2) Li, Z.; Tan, S.; Li, S.; Shen, Q.; Wang, K. Cancer Drug Delivery in the Nano Era: An Overview and Perspectives (Review). *Oncol. Rep.* **2017**, *38* (2), 611–624. https://doi.org/10.3892/or.2017.5718.

(3) Arunkumar, E.; Forbes, C. C.; Smith, B. D. Improving the Properties of Organic Dyes by Molecular Encapsulation. *Eur. J. Org. Chem.* **2005**, No. 19, 4051–4059. https://doi.org/10.1002/ejoc.200500372.

(4) Steichen, S. D.; Caldorera-Moore, M.; Peppas, N. A. A Review of Current Nanoparticle and Targeting Moieties for the Delivery of Cancer Therapeutics. *Eur. J. Pharm. Sci.* **2013**, *48* (3), 416–427. https://doi.org/10.1016/J.EJPS.2012.12.006.

(5) Kang, H.; Rho, S.; Stiles, W. R.; Hu, S.; Baek, Y.; Hwang, D. W.; Kashiwagi, S.; Kim, M. S.; Choi, H. S. Size-Dependent EPR Effect of Polymeric Nanoparticles on Tumor Targeting. *Adv. Healthcare Mater.* **2020**, *9* (1), 1901223. https://doi.org/10.1002/adhm.201901223.

(6) Bulbake, U.; Doppalapudi, S.; Kommineni, N.; Khan, W. Liposomal Formulations in Clinical

Use: An Updated Review. *Pharmaceutics*. **2017**, *9* (2), 12. https://doi.org/10.3390/pharmaceutics9020012.

(7) Tao, L.; Chan, J. W.; Uhrich, K. E. Drug Loading and Release Kinetics in Polymeric Micelles: Comparing Dynamic versus Unimolecular Sugar-Based Micelles for Controlled Release. *J. Bioact. Compat. Polym.* **2016**, *31* (3), 227–241. https://doi.org/10.1177/0883911515609814.

(8) Zhou, W.; Li, C.; Wang, Z.; Zhang, W.; Liu, J. Factors Affecting the Stability of Drug-Loaded Polymeric Micelles and Strategies for Improvement. *J. Nanopart. Res.* **2016**, *18* (9), 275. https://doi.org/10.1007/s11051-016-3583-y.

(9) Popeney, C. S.; Lukowiak, M. C.; Böttcher, C.; Schade, B.; Welker, P.; Mangoldt, D.; Gunkel, G.; Guan, Z.; Haag, R. Tandem Coordination, Ring-Opening, Hyperbranched Polymerization for the Synthesis of Water-Soluble Core-Shell Unimolecular Transporters. *ACS Macro Lett.* **2012**, *1* (5), 564–567. https://doi.org/10.1021/mz300083y.

(10) Zhang, L.; Liu, W.; Lin, L.; Chen, D.; Stenzel, M. H. Degradable Disulfide Core-Cross-Linked Micelles as a Drug Delivery System Prepared from Vinyl Functionalized Nucleosides via the RAFT Process. *Biomacromolecules* **2008**, *9* (11), 3321–3331. https://doi.org/10.1021/bm800867n.

(11) Kim, J. O.; Kabanov, A. V.; Bronich, T. K. Polymer Micelles with Cross-Linked Polyanion Core for Delivery of a Cationic Drug Doxorubicin. *J. Controlled Release* **2009**, *138* (3), 197–204. https://doi.org/10.1016/J.JCONREL.2009.04.019.

(12) Cajot, S.; Lautram, N.; Passirani, C.; Jérôme, C. Design of Reversibly Core Cross-Linked Micelles Sensitive to Reductive Environment. *J. Controlled Release* **2011**, *152* (1), 30–36. https://doi.org/10.1016/J.JCONREL.2011.03.026.

(13) Zhang, X.; Ai, C.; Ma, J.; Xu, J.; Yang, S. Synthesis of Zwitterionic Shell Cross-Linked Micelles with PH-Dependent Hydrophilicity. *J. Colloid Interface Sci.* **2011**, *356* (1), 24–30.

https://doi.org/10.1016/J.JCIS.2010.12.041.

(14) Fa, S.; Zhao, Y. General Method for Peptide Recognition in Water through Bioinspired Complementarity. *Chem. Mater.* **2019**, *31* (13), 4889–4896. https://doi.org/10.1021/acs.chemmater.9b01613.

(15) Awino, J. K.; Hu, L.; Zhao, Y. Molecularly Responsive Binding through Co-Occupation of Binding Space: A Lock-Key Story. *Org. Lett.* **2016**, *18* (7), 1650–1653. https://doi.org/10.1021/acs.orglett.6b00527.

(16) Hennig, R.; Veser, A.; Kirchhof, S.; Goepferich, A. Branched Polymer-Drug Conjugates for Multivalent Blockade of Angiotensin II Receptors. *Mol. Pharmaceutics.* **2015**, *12* (9), 3292–3302. https://doi.org/10.1021/acs.molpharmaceut.5b00301.

(17) Elkin, I.; Banquy, X.; Barrett, C. J.; Hildgen, P. Non-Covalent Formulation of Active Principles with Dendrimers: Current State-of-the-Art and Prospects for Further Development. *J. Controlled Release* **2017**, *264*, 288–305. https://doi.org/10.1016/j.jconrel.2017.09.002.

(18) Lukowiak, M. C.; Thota, B. N. S.; Haag, R. Dendritic Core–Shell Systems as Soft Drug Delivery Nanocarriers. *Biotechnol. Adv.* **2015**, *33* (6), 1327–1341. https://doi.org/10.1016/J.BIOTECHADV.2015.03.014.

(19) Fan, X.; Li, Z.; Loh, X. J. Recent Development of Unimolecular Micelles as Functional Materials and Applications. *Polym. Chem.* **2016**, *7* (38), 5898–5919. https://doi.org/10.1039/C6PY01006G.

(20) Qin, M.; Zong, H.; Kopelman, R. Click Conjugation of Peptide to Hydrogel Nanoparticles for Tumor-Targeted Drug Delivery. *Biomacromolecules* **2014**, *15* (10), 3728–3734. https://doi.org/10.1021/bm501028c.

(21) Wu, L.; Zhang, Y.; Li, Z.; Yang, G.; Kochovski, Z.; Chen, G.; Jiang, M. “sweet” Architecture-Dependent Uptake of Glycocalyx-Mimicking Nanoparticles Based on Biodegradable

Aliphatic Polyesters by Macrophages. *J. Am. Chem. Soc.* **2017**, *139* (41), 14684–14692. https://doi.org/10.1021/jacs.7b07768.

(22) Glass, J. J.; Chen, L.; Alcantara, S.; Crampin, E. J.; Thurecht, K. J.; De Rose, R.; Kent, S. J. Charge Has a Marked Influence on Hyperbranched Polymer Nanoparticle Association in Whole Human Blood. *ACS Macro Lett.* **2017**, *6* (6), 586–592. https://doi.org/10.1021/acsmacrolett.7b00229.

(23) Moorefield, C. N.; Newkome, G. R. Unimolecular Micelles: Supramolecular Use of Dendritic Constructs to Create Versatile Molecular Containers. *C. R. Chim.* **2003**, *6* (8–10), 715–724. https://doi.org/10.1016/J.CRCI.2003.04.002.

(24) Mou, Q.; Ma, Y.; Jin, X.; Yan, D.; Zhu, X. Host-Guest Binding Motifs Based on Hyperbranched Polymers. *Chem. Commun.* **2016**, *52* (79), 11728–11743. https://doi.org/10.1039/c6cc03643k.

(25) Cao, X.; Shi, Y.; Wang, X.; Graff, R. W.; Gao, H. Design a Highly Reactive Trifunctional Core Molecule To Obtain Hyperbranched Polymers with over a Million Molecular Weight in One-Pot Click Polymerization. *Macromolecules* **2016**, *49* (3), 760–766. https://doi.org/10.1021/acs.macromol.5b02678.

(26) Jeon, I.-Y.; Noh, H.-J.; Baek, J.-B. Hyperbranched Macromolecules: From Synthesis to Applications. *Molecules* **2018**, *23* (3). https://doi.org/10.3390/MOLECULES23030657.

(27) Wang, D.; Zhao, T.; Zhu, X.; Yan, D.; Wang, W. Bioapplications of Hyperbranched Polymers. *Chem. Soc. Rev.* **2015**, *44* (12), 4023–4071. https://doi.org/10.1039/C4CS00229F.

(28) Ban, Q.; Sun, W.; Kong, J.; Wu, S. Hyperbranched Polymers with Controllable Topologies for Drug Delivery. *Chem. - Asian J.* **2018**, *13* (22), 3341–3350. https://doi.org/10.1002/asia.201800812.

(29) Misri, R.; Wong, N. K. Y.; Shenoi, R. A.; Lum, C. M. W.; Chafeeva, I.; Toth, K.; Rustum, Y.;

Kizhakkedathu, J. N.; Khan, M. K. Investigation of Hydrophobically Derivatized Hyperbranched Polyglycerol with PEGylated Shell as a Nanocarrier for Systemic Delivery of Chemotherapeutics. *Nanomedicine* **2015**, *11* (7), 1785–1795. https://doi.org/10.1016/J.NANO.2015.04.016.

(30) Geyik, C.; Ciftci, M.; Demir, B.; Guler, B.; Ozkaya, A. B.; Gumus, Z. P.; Barlas, F. B.; Odaci Demirkol, D.; Coskunol, H.; Timur, S.; Yagci, Y. Controlled Release of Anticancer Drug Paclitaxel Using Nano-Structured Amphiphilic Star-Hyperbranched Block Copolymers. *Polym. Chem.* **2015**, *6* (30), 5470–5477. https://doi.org/10.1039/c5py00780a.

(31) Cao, X.; Shi, Y.; Gan, W.; Gao, H. Tandem Functionalization in a Highly Branched Polymer with Layered Structure. *Chem. - Eur. J.* **2018**, *24* (22), 5974–5981. https://doi.org/10.1002/chem.201800683.

(32) Shi, Y.; Graff, R. W.; Cao, X.; Wang, X.; Gao, H. Chain-Growth Click Polymerization of AB2 Monomers for the Formation of Hyperbranched Polymers with Low Polydispersities in a One-Pot Process. *Angew. Chem. Int. Ed. Engl.* **2015**, *54* (26), 7631–7635. https://doi.org/10.1002/anie.201502578.

(33) Shi, Y.; Cao, X.; Gao, H. The Use of Azide–Alkyne Click Chemistry in Recent Syntheses and Applications of Polytriazole-Based Nanostructured Polymers. *Nanoscale* **2016**, *8* (9), 4864–4881. https://doi.org/10.1039/C5NR09122E.

(34) Cao, X.; Shi, Y.; Gao, H. A Novel Chain-Growth CuAAC Polymerization: One-Pot Synthesis of Dendritic Hyperbranched Polymers with Well-Defined Structures. *Synlett* **2016**, *28* (4), 391–396. https://doi.org/10.1055/s-0036-1588684.

(35) Kolb, H. C.; Finn, M. G.; Sharpless, K. B. Click Chemistry: Diverse Chemical Function from a Few Good Reactions. *Angew. Chem. Int. Ed. Engl.* **2001**, *40* (11), 2004–2021. https://doi.org/10.1002/1521-3773(20010601)40:11<2004::AID-ANIE2004>3.0.CO;2-5.

(36) Zou, L.; Shi, Y.; Cao, X.; Gan, W.; Wang, X.; Graff, R. W.; Hu, D.; Gao, H. Synthesis of

Acid-Degradable Hyperbranched Polymers by Chain-Growth CuAAC Polymerization of an AB3 Monomer. *Polym. Chem.* **2016**, *7* (35), 5512–5517. https://doi.org/10.1039/c6py01265e.

(37) Cavestri, R. C.; Fedor, L. R. Base-Catalyzed β-Elimination Reactions in Aqueous Solution. IV. Elimination from 4-(4-Substituted Benzoyloxy)-2-Butanones. *J. Am. Chem. Soc.* **1970**, *92* (15), 4610–4613.

(38) Koulov, A. V.; Hanshaw, R. G.; Stucker, K. A.; Lakshmi, C.; Smith, B. D. Biophysical Studies of a Synthetic Mimic of the Apoptosis-Detecting Protein Annexin V. *Isr. J. Chem.* **2005**, *45* (3), 373–379. https://doi.org/10.1560/6AD4-LC9G-P57M-BE5Y.

(39) Jarvis, T. S.; Roland, F. M.; Dubiak, K. M.; Huber, P. W.; Smith, B. D. Time-Lapse Imaging of Cell Death in Cell Culture and Whole Living Organisms Using Turn-on Deep-Red Fluorescent Probes. *J. Mater. Chem. B* **2018**, *6* (30), 4963–4971. https://doi.org/10.1039/C8TB01495G.

(40) Ojida, A.; Honda, K.; Shinmi, D.; Kiyonaka, S.; Mori, Y.; Hamachi, I. Oligo-Asp Tag/Zn(II) Complex Probe as a New Pair for Labeling and Fluorescence Imaging of Proteins. *J. Am. Chem. Soc.* **2006**, *128* (32), 10452–10459. https://doi.org/10.1021/ja0618604.

(41) Johnson, J. R.; Jiang, H.; Smith, B. D. Zinc(II)-Coordinated Oligotyrosine: A New Class of Cell Penetrating Peptide. *Bioconjugate Chem.* **2008**, *19* (5), 1033–1039. https://doi.org/10.1021/bc700466z.

(42) Schulze, B.; Schubert, U. S. Beyond Click Chemistry-Supramolecular Interactions of 1,2,3-Triazoles. *Chem. Soc. Rev.* **2014**, *43* (8), 2522–2571. https://doi.org/10.1039/c3cs60386e.

(43) Kumar, P.; Hornum, M.; Nielsen, L. J.; Enderlin, G.; Andersen, N. K.; Len, C.; Hervé, G.; Sartori, G.; Nielsen, P. High-Affinity RNA Targeting by Oligonucleotides Displaying Aromatic Stacking and Amino Groups in the Major Groove. Comparison of Triazoles and Phenyl Substituents. *J. Org. Chem.* **2014**, *79* (7), 2854–2863.

https://doi.org/10.1021/jo4025896.

(44) Riccardi, C.; Nicoletti, I. Analysis of Apoptosis by Propidium Iodide Staining and Flow Cytometry. *Nat. Protoc.* **2006**, *1* (3), 1458–1461. https://doi.org/10.1038/nprot.2006.238.

(45) Bucevičius, J.; Lukinavičius, G.; Gerasimaitė, R. The Use of Hoechst Dyes for DNA Staining and Beyond. *Chemosensors* **2018**, *6* (2), 18. https://doi.org/10.3390/chemosensors6020018.

(46) Żurek-Biesiada, D.; Waligórski, P.; Dobrucki, J. W. UV-Induced Spectral Shift and Protonation of DNA Fluorescent Dye Hoechst 33258. *J. Fluoresc.* **2014**, *24* (6), 1791–1801. https://doi.org/10.1007/s10895-014-1468-y.

(47) Ladinig, M.; Leupin, W.; Meuwly, M.; Respondek, M.; Wirz, J.; Zoete, V. Protonation Equilibria of Hoechst 33258 in Aqueous Solution. *Helv. Chim. Acta* **2005**, *88* (1), 53–67.

(48) Alemán, C.; Namba, A. M.; Casanovas, J. Acid-Base and Electronic Structure-Dependent Properties of Hoechst 33342. *J. Biomol. Struct. Dyn.* **2005**, *23* (1), 29–36. https://doi.org/10.1080/07391102.2005.10507044.

(49) Cunningham, A. J.; Robinson, M.; Banquy, X.; Leblond, J.; Zhu, X. X. Bile Acid-Based Drug Delivery Systems for Enhanced Doxorubicin Encapsulation: Comparing Hydrophobic and Ionic Interactions in Drug Loading and Release. *Mol. Pharmaceutics* **2018**, *15* (3), 1266–1276. https://doi.org/10.1021/acs.molpharmaceut.7b01091.

(50) Bell, D. H. Characterization of the Fluorescence of the Antitumor Agent, Mitoxantrone. *Biochim. Biophys. Acta, Gene Struct. Expression* **1988**, *949* (1), 132–137. https://doi.org/10.1016/0167-4781(88)90063-2.

(51) Jares-Erijman, E. A.; Jovin, T. M. FRET Imaging. *Nat. Biotechnol.* **2002**, *21*, 1387–1395. https://doi.org/10.1038/nbt896.

(52) Breuzard, G.; El-Khoury, V.; Millot, C.; Manfait, M.; Millot, J. M. Energy Transfer to Analyse Membrane-Integrated Mitoxantrone in BCRP-Overexpressed Cells. *J. Photochem.*

Photobiol., B **2007**, *87* (2), 113–123. https://doi.org/10.1016/j.jphotobiol.2007.03.001.

(53) Cheng, J.-G.; Yu, H.-J.; Chen, Y.; Liu, Y. Selective Binding and Controlled Release of Anticancer Drugs by Polyanionic Cyclodextrins. *Bioorg. Med. Chem.* **2018**, *26* (9), 2287–2290. https://doi.org/10.1016/j.bmc.2018.03.013.

(54) Zhu, D.; Fan, F.; Huang, C.; Zhang, Z.; Qin, Y.; Lu, L.; Wang, H.; Jin, X.; Zhao, H.; Yang, H.; Zhang, C.; Yang, J.; Liu, Z.; Sun, H.; Leng, X.; Kong, D.; Zhang, L. Bubble-Generating Polymersomes Loaded with Both Indocyanine Green and Doxorubicin for Effective Chemotherapy Combined with Photothermal Therapy. *Acta Biomater.* **2018**, *75*, 386–397. https://doi.org/10.1016/j.actbio.2018.05.033.

(55) Klymchenko, A. S. Solvatochromic and Fluorogenic Dyes as Environment-Sensitive Probes: Design and Biological Applications. *Acc. Chem. Res.* **2017**, *50* (2), 366–375. https://doi.org/10.1021/acs.accounts.6b00517.

(56) Yang, Z.; He, Y.; Lee, J. H.; Chae, W. S.; Ren, W. X.; Lee, J. H.; Kang, C.; Kim, J. S. A Nile Red/BODIPY-Based Bimodal Probe Sensitive to Changes in the Micropolarity and Microviscosity of the Endoplasmic Reticulum. *Chem. Commun.* **2014**, *50* (79), 11672–11675. https://doi.org/10.1039/c4cc04915b.

(57) Venditto, V. J.; Simanek, E. E. Cancer Therapies Utilizing the Camptothecins: A Review of the in Vivo Literature. *Mol. Pharmaceutics* **2010**, *7* (2), 307–349. https://doi.org/10.1021/mp900243b.

(58) Venditto, V. J.; Szoka, F. C. Cancer Nanomedicines: So Many Papers and so Few Drugs! *Adv. Drug Delivery Rev*. **2013**, *65* (1), 80–88. https://doi.org/10.1016/j.addr.2012.09.038.

(59) Lai, C. H.; Chang, C. C.; Weng, Y. L.; Chuang, T. H. Synthesis, Experimental and Density Functional Theory (DFT) Studies on Solubility of Camptothecin Derivatives. *Molecules* **2018**, *23* (12), 3170. https://doi.org/10.3390/molecules23123170.

(60) Han, X.; Liu, D.-E.; Wang, T.; Lu, H.; Ma, J.; Chen, Q.; Gao, H. Aggregation-Induced-

Emissive Molecule Incorporated into Polymeric Nanoparticulate as FRET Donor for Observing Doxorubicin Delivery. *ACS Appl. Mater. Interfaces* **2015**, *7* (42), 23760–23766. https://doi.org/10.1021/acsami.5b08202.

(61) Cabral, H.; Matsumoto, Y.; Mizuno, K.; Chen, Q.; Murakami, M.; Kimura, M.; Terada, Y.; Kano, M. R.; Miyazono, K.; Uesaka, M.; Nishiyama, N.; Kataoka, K. Accumulation of Sub-100 Nm Polymeric Micelles in Poorly Permeable Tumours Depends on Size. *Nat. Nanotechnol.* **2011**, *6* (12), 815–823. https://doi.org/10.1038/nnano.2011.166.

(62) Blanco, E.; Shen, H.; Ferrari, M. Principles of Nanoparticle Design for Overcoming Biological Barriers to Drug Delivery. *Nat. Biotechnol.* **2015**, *33* (9), 941–951. https://doi.org/10.1038/nbt.3330.

GRAPHICAL ABSTRACT

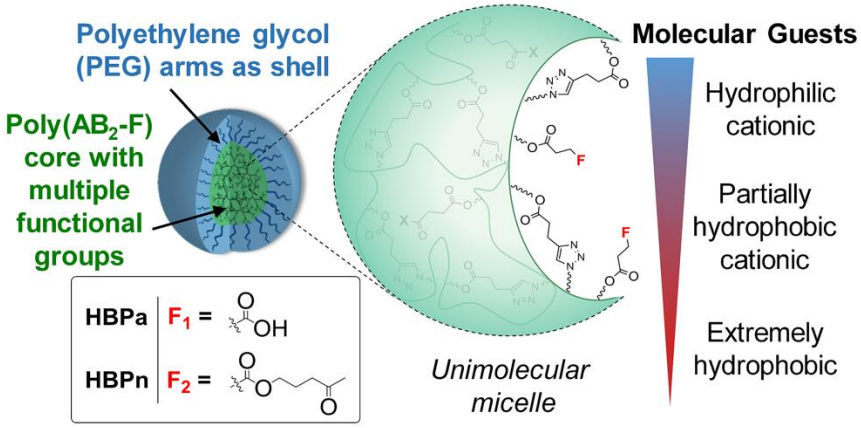

For Table of Contents Only